Quantum theory of the diamond maser: Stimulated and superradiant emission

Christoph W. Zollitsch [1,2] and Jonathan D. Breeze [1,*]

[1]*Department of Physics and Astronomy, University College London, Gower Street, London WC1E 6BT, United Kingdom*

[2]*Department of Chemistry, Saarland University, 66123 Saarbrücken, Germany*

(Received 10 October 2024; accepted 25 April 2025; published 14 May 2025)

We present a quantum theory of diamond masers operating at any temperature using a cavity quantum electrodynamical framework. Special attention is paid to the recently demonstrated room-temperature solid-state masers based on nitrogen-vacancy (NV) defect centers in diamond, but the model can easily be modified for other photoexcited chromophores such as pentacene-doped paraterphenyl, vacancies in silicon-carbide or boron nitride. We show that the eight energy levels involved in the optically pumped NV center polarization process can be mapped to a simple pumped two-level-system. We then derive simple analytical expressions for the optical pump threshold condition for masing as well as the steady-state microwave output power which can be used to design and predict maser performance. Finally, we investigate second-order correlations and find that typical diamond masers operate in an intermediate regime between the good and bad cavity limits where photon emission is driven by both stimulated and superradiant processes.

DOI: 10.1103/PhysRevA.111.053714

I. INTRODUCTION

After its invention in 1954 [1], the maser became a vital technology for deep-space communication, radio astronomy, and time-keeping due to its unparalleled ultralow noise and frequency stability [2–4]. However, the spectrum of maser applications was narrow due to reliance on bulky cryogenic and high-vacuum systems. With the recent realization of solid-state maser oscillators at room-temperature and ambient pressure [5,6], masers could become integral to radio-frequency and microwave systems and find application in quantum computing, communications, sensing, medicine, and security. There has been a flurry of experimental work on solid-state room-temperature maser amplifiers [7–9], mode coolers [10–14], and alternative gain media [15] yet theoretical investigation has been less active. The room-temperature diamond maser [6] and subsequent experimental work was motivated by the seminal theoretical proposal by Jin *et al.* [16]. Although this work proposed a room-temperature maser, the theory was only valid for very low temperatures, resulting in overestimation of pump rates required to achieve a sufficient population inversion for masing. Here we present a diamond maser theory that is valid at any temperature and can be modified for alternative gain media. We analyze steady-state dynamics up to second-order correlations to derive simple expressions for the maser threshold, cavity photon population, output power, and propose design criteria for maser performance. Finally, we discuss spin-photon and spin-spin correlation, and find that microwave photon emission is a combination of superradiant and stimulated emission, with spontaneous emission playing a lesser role. Our findings provide a comprehensive theoretical framework for future solid-state maser research and highlight the importance of many-body correlations.

II. POPULATION DYNAMICS OF PUMPED NV CENTERS

The electronic ground-state $^3A_2$ of a charged nitrogen-vacancy (NV^-) defect in diamond is a spin-triplet ($S = 1$) [17]. The $|m_s = \pm 1\rangle$ sublevels are quasidegenerate and lie approximately 2.87 GHz above the $|m_s = 0\rangle$ sublevel, characterized by the zero-field splitting parameter D. The degeneracy of the $|m_s = \pm 1\rangle$ levels can be lifted by strain or an externally applied static magnetic field B_0. In the following we will neglect strain effects and focus on the Zeeman effect for tuning the energy levels. Figure 1(a) shows the energy level diagram for the electronic ground and first excited states of NV^- centers in diamond at zero magnetic field and finite field applied along a $\langle 111\rangle$ NV defect axis. The ground-state triplet $^3A_2$ population can be optically pumped into the excited-state triplet by light of wavelength shorter than the zero-phonon line, $\lambda < 640$ nm. Typically, laser light of $\lambda \sim 532$ nm is used due to a local maximum of the absorption coefficient [18]. Electrons in the $|m_s = \pm 1\rangle$ sublevels undergo spin-selective intersystem crossing into metastable singlet states $^1A_1$ which rapidly relax to ^1E singlet states, then subsequently decay to the ground-state triplets. The spin selective intersystem crossing results in preferential population of the $|m_s = 0\rangle$ sublevels. Under sustained optical pumping a steady-state non-Boltzmann population is established with excess population in the ground state $|m_s = 0\rangle$ sublevel. Masing requires a population inversion between the $|m_s = 0\rangle$ and $|m_s = -1\rangle$

*Contact author: j.breeze@ucl.ac.uk

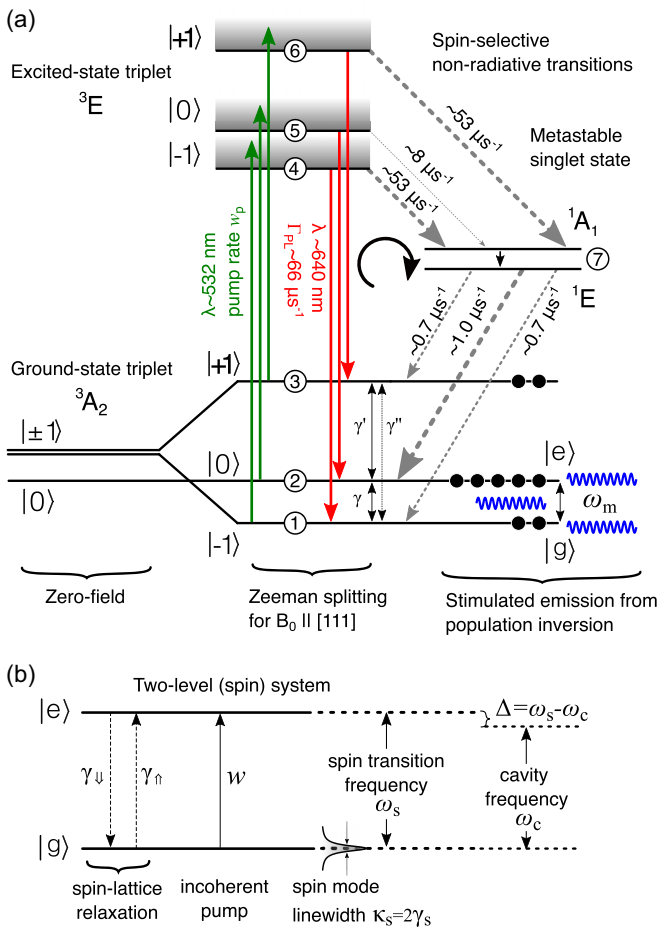

FIG. 1. Energy levels of NV center and cavity-coupled spins. (a) Energy diagram depicting the energy levels involved in the spin population dynamics of photoexcited NV$^-$ centers. The ground-state and excited spin-triplet sublevels are labeled 1 to 6 in order of increasing energy when sufficient external magnetic field ($B_0 >$ 102.5 mT) is applied and the metastable singlet states can be regarded as a single level since the decay rate $^1A_1 \mapsto {}^1E$ is faster than other processes. (b) Simplified model for incoherently pumped spins coupled to a cavity.

sublevels. Under continuous pumping, this condition is fulfilled when $|m_s = -1\rangle$ is Zeeman shifted below $|m_s = 0\rangle$ by a magnetic field B_0 (parallel to a NV ⟨111⟩ axis). An ensemble in an inverted state can be brought into emission by matching the energy difference of the $|m_s = 0\rangle$ and $|m_s = -1\rangle$ sublevels to microwave photons in a resonant cavity [Fig. 1(a)].

Focusing on the two sublevels active during masing, ground state $|g\rangle \equiv |m_s = -1\rangle$ and excited state $|e\rangle \equiv |m_s = 0\rangle$, it can be shown (see the Appendix) that the full eight-level energy level scheme in Fig. 1(a) can be directly mapped onto the simpler two-level system shown in Fig. 1(b) with $w = \eta w_{\rm opt}$, the effective pump rate of the two-level system is proportional to the NV-center optical pump rate $w_{\rm opt}$ through a pump efficiency η. The inversion of the pumped two-level system is then given by $\sigma^z = (1 + \gamma/\eta w_{\rm opt})^{-1} = (1 + \gamma/w)^{-1}$. This expression is only valid if the spin-triplet states are pure with no mixing between them. State mixing of excited triplet sublevels leads to non-zero intersystem crossing rates into $^1A_1$ from the excited $|m_s = 0\rangle$ sublevel, reducing spin-selectivity and spin polarization. This can be accounted for by scaling the inversion, $\sigma^z = \xi(1 + \gamma/\eta w_{\rm opt})^{-1}$, where parameter $\xi = 1$ for zero mixing and $\xi < 1$ otherwise. Mixing can be caused by misalignment of the magnetic field B_0 with respect to the NV$^-$ defect axis [19,20]. The parameters η and ξ can be determined by fitting the two-level inversion equation to the inversion obtained from the full set of rate equations [8,19], including all NV$^-$ energy levels involved in the optical pumping process (see the Appendix). The rates of spin-lattice relaxation, fluorescence decay and intersystem crossing are given in Fig. 1(a) for the individual transitions. Note, we assume equal rates of the spin-lattice relaxation for phonon driven decay and excitation ($\gamma_\Downarrow = \gamma_\Uparrow$) which is approximately true for high temperatures where $\hbar\omega_s \ll k_B T$. Mapping the full NV energy level scheme onto a two-level system in this way enables a simple theory to be developed that analytically predicts maser parameters crucial for the design and development of new and improved maser devices. In the remainder of the discussion, we assume a perfect alignment of B_0 to a ⟨111⟩ NV$^-$ defect axis to retain pure spin states. Note that misalignment will formally not change the analytical results, only affecting the final absolute values for masing threshold pump rate and microwave output power.

III. MICROWAVE CAVITY

The cavity provides the basis for resonant emission from the spin ensemble. To achieve stable and continuous emission of microwave power the cavity losses need to be low. The figure of merit describing cavity losses is the quality factor, defined by $Q = \omega_c/2\kappa$, where ω_c is the resonant frequency and κ is the (half-width) linewidth. The measured linewidth is the sum of the intrinsic loss rate κ_0 due to resistive, dielectric, and radiative losses and κ_e, the coupling of the cavity to external circuitry: $\kappa = \kappa_0 + \kappa_e$. The degree of external coupling is characterized by a coupling factor $\beta = \kappa_e/\kappa_0$. The cavity is overcoupled if $\beta > 1$, undercoupled for $\beta < 1$ and critically coupled for $\beta = 1$. In the latter case, external circuity is impedance matched to the cavity, allowing for optimal energy transfer.

IV. MASTER EQUATION: TAVIS-CUMMINGS HAMILTONIAN

Consider an ensemble of $j = 1, \ldots, N$ spins with transition frequencies ω_s between the $|g\rangle$ and $|e\rangle$ states of the reduced two-level system of the NV centers if a magnetic field of $B_0 > \gamma_e D \sim 102.5$ mT is applied along a ⟨111⟩ crystal axis [as shown in Fig. 1(b)] where γ_e is the gyromagnetic ratio for NV$^-$ electron spins. Each spin with frequency $\omega_s = \gamma_e B_0 - D$ is coupled to the cavity mode of frequency ω_c by a single-spin–single-photon coupling rate g. The coherent dynamics of this system can be described by the Tavis-Cummings Hamiltonian (under rotating-wave approximation) [21,22]:

$$\mathcal{H} = \hbar\omega_c \hat{a}^\dagger \hat{a} + \frac{1}{2}\hbar\omega_s \sum_{j=1}^{N} \hat{\sigma}_j^z + \hbar g \sum_{j=1}^{N} (\hat{\sigma}_j^+ \hat{a} + \hat{\sigma}_j^- \hat{a}^\dagger), \quad (1)$$

where $\hat{a}^\dagger(\hat{a})$ are cavity-field creation (annihilation) operators, $\hat{\sigma}_j^+ = |e_j\rangle\langle g_j|$ and $\hat{\sigma}_j^- = |g_j\rangle\langle e_j|$ are the spin raising and lowering operators for the jth spin, and $\hat{\sigma}_j^z = [\hat{\sigma}_j^+, \hat{\sigma}_j^-] = |e_j\rangle\langle e_j| - |g_j\rangle\langle g_j|$ is the inversion operator. The first and second terms describe the uncoupled cavity resonator and the ensemble of spins. The third term is the sum of individual interactions between spins and cavity photons, where g is assumed to be homogeneous for all spins. The coupling strength is $g = \mathbf{B}_{\rm vac}\boldsymbol{\mu}/\hbar = \gamma_{\rm e}\sqrt{\mu_0\hbar\omega_{\rm c}/2V_m}$, where $\mathbf{B}_{\rm vac}$ is the oscillating vacuum magnetic field in the cavity, $\boldsymbol{\mu}$ is the magnetic moment of the spin, μ_0 is the free-space magnetic permeability, and $V_{\rm m}$ is the magnetic mode volume of the cavity.

The time derivative of the expectation value of an operator $\hat{o}$ can be found by taking the trace of the operator acting upon the time derivative of the reduced density matrix ρ, $d\langle\hat{o}\rangle/dt = {\rm Tr}(\hat{o}\dot{\rho})$ where $\dot{\rho} = (i\hbar)^{-1}[\mathcal{H},\rho] + \mathcal{L}[\rho]$. The Liouvillian $\mathcal{L}[\rho] = \mathcal{L}_{\rm c}[\rho] + \mathcal{L}_{\rm ph}[\rho] + \mathcal{L}_{\rm s}[\rho] + \mathcal{L}_{\rm w}[\rho]$ accounts for the dissipative and incoherent processes of cavity decay, phonon-induced spin-lattice relaxation, spin dephasing, and pumping, respectively, given by $\mathcal{L}_{\rm c}[\rho] = \kappa(\bar{n}+1)\mathcal{D}[\hat{a}]\rho + \kappa\bar{n}\mathcal{D}[\hat{a}^\dagger]\rho$, $\mathcal{L}_{\rm ph}[\rho] = \frac{1}{2}\sum_{j=1}^{N}(\gamma_\Downarrow\mathcal{D}[\hat{\sigma}_j^-]\rho + \gamma_\Uparrow\mathcal{D}[\hat{\sigma}_j^+]\rho)$, $\mathcal{L}_{\rm s}[\rho] = \frac{\gamma_\perp}{4}\sum_{j=1}^{N}\mathcal{D}[\hat{\sigma}_j^z]\rho$, and $\mathcal{L}_{\rm w}[\rho] = \frac{w}{2}\sum_{j=1}^{N}\mathcal{D}[\hat{\sigma}_j^+]\rho$ where $\mathcal{D}[\hat{o}]\rho = 2\hat{o}\rho\hat{o}^\dagger - \{\hat{o}^\dagger\hat{o},\rho\}$ is the Lindblad superoperator and $\bar{n}$ is the mean number of thermal photons in the cavity given by Bose-Einstein statistics as $\bar{n} = [\exp(\hbar\omega_{\rm c}/k_{\rm B}T) - 1]^{-1}$. $\gamma_\perp = 1/T_2^*$ describes the spin dephasing rate (half-width linewidth) and $\gamma_\Downarrow$ and $\gamma_\Uparrow$ are the temperature-dependent rates of phonon-induced [23] relaxation and excitation, respectively. For temperatures $T \ll \hbar\omega_{\rm s}/k_{\rm B}$, the excitation probability becomes negligible, $\gamma_\Uparrow \to 0$. Here we consider maser operation at room temperature, where $\gamma_\Downarrow \sim \gamma_\Uparrow \sim \gamma/2$ and $\gamma = 1/T_1$ is given by the spin-lattice relaxation time T_1, but the theory can be applied to any temperature if T_1 is known.

V. FIRST-ORDER DYNAMICAL EQUATIONS

Using the Hamiltonian in Eq. (1) and the Liouvillian a closed set of first-order optical-Bloch equations can be derived [24,25] using the mean-field approximation $\langle ab\rangle \approx \langle a\rangle\langle b\rangle$, collective spin operators defined by $\hat{S}^\pm = \sum_j^N \hat{\sigma}_j^\pm = N\hat{\sigma}_j^\pm$, $\hat{S}^z = \sum_j^N \hat{\sigma}_j^z = N\hat{\sigma}_j^z$, and assuming $\kappa, \gamma_\perp \gg \gamma, w$:

$$\langle\dot{a}\rangle = -(i\omega_{\rm c} + \kappa)\langle a\rangle - ig\langle S^-\rangle, \tag{2}$$

$$\langle\dot{S}^-\rangle = -(i\omega_s + \gamma_\perp)\langle S^-\rangle + ig\langle a\rangle\langle S^z\rangle, \tag{3}$$

$$\langle\dot{S}^z\rangle = wN - (w+\gamma)\langle S^z\rangle - 2ig(\langle S^+\rangle\langle a\rangle - \langle a^\dagger\rangle\langle S^-\rangle). \tag{4}$$

VI. INVERSION, COOPERATIVITY, AND PUMP THRESHOLD

Assuming a harmonic time dependence for the cavity field $\langle a(t)\rangle = \langle a\rangle e^{-i\omega t}$ and transverse collective spin polarization $\langle S^-(t)\rangle = \langle S^-\rangle e^{-i\omega t}$, we can rewrite Eqs. (2) and (3) to yield

$$\langle a\rangle = -ig\langle S^-\rangle[\kappa + i(\omega_{\rm c} - \omega)]^{-1}, \tag{5}$$

$$\langle S^-\rangle = +ig\langle a\rangle\langle S^z\rangle[\gamma_\perp + i(\omega_{\rm s} - \omega)]^{-1}. \tag{6}$$

Substituting Eq. (5) into Eq. (6), we can derive an expression for the collective spin inversion

$$\langle S^z\rangle = g^{-2}[\kappa + i(\omega_{\rm c} - \omega)][\gamma_\perp + i(\omega_{\rm s} - \omega)], \tag{7}$$

which must be real-valued. Equating the imaginary part to zero, $(\omega_{\rm c} - \omega)\gamma_\perp + (\omega_{\rm s} - \omega)\kappa = 0$, and solving for frequency ω reveals the maser frequency $\omega_{\rm m} = (\omega_{\rm c}\gamma_\perp + \omega_{\rm s}\kappa)/(\gamma_\perp + \kappa)$. Substitution of the maser frequency into Eq. (7) yields the above-threshold inversion

$$\langle S^z\rangle = \frac{\kappa\gamma_\perp}{g^2}(1 + \Delta^2), \tag{8}$$

where $\Delta = (\omega_{\rm c} - \omega_{\rm s})/(\kappa + \gamma_\perp)$ is a cavity-spin detuning parameter. At resonance ($\omega_{\rm c} = \omega_{\rm s}$, $\Delta = 0$) and above threshold the inversion is $\langle S^z\rangle = \kappa\gamma_\perp/g^2$. Substitution of the maser frequency into the equations for the cavity field $\langle a\rangle$ in Eq.(5) and transverse spin polarization $\langle S^-\rangle$ in Eq. (6) yields

$$\langle a\rangle = -ig\langle S^-\rangle[\kappa(1 + i\Delta)]^{-1}, \tag{9}$$

$$\langle S^-\rangle = +ig\langle a\rangle\langle S^z\rangle[\gamma_\perp(1 - i\Delta)]^{-1}. \tag{10}$$

Examining the last term of the equation of motion for $\langle S^z\rangle$ in Eq. (4) and substituting $\langle S^-\rangle$ in Eq. (10) and its complex conjugate $\langle S^+\rangle$, we find it is proportional to the cavity photon population $n_{\rm c} = \langle a^\dagger\rangle\langle a\rangle \equiv |a|^2$:

$$2ig(\langle S^+\rangle\langle a\rangle - \langle a^\dagger\rangle\langle S^-\rangle) = \frac{4g^2\langle S^z\rangle n_{\rm c}}{\gamma_\perp(1 + \Delta^2)}, \tag{11}$$

and equal to twice the net microwave photon emission rate since the inversion changes by two upon emission of one photon. The maser pump threshold $w_{\rm thr}$ is derived by requiring a steady-state cavity photon number greater than zero ($n_{\rm c} > 0$). Combining Eq. (11) with Eq. (4) the condition is found to be $w > \gamma/(N/\langle S^z\rangle - 1)$. We identify the term $N/\langle S^z\rangle$ as the collective cooperativity C:

$$C = \frac{N}{\langle S^z\rangle} = \frac{g^2N}{\kappa\gamma_\perp}(1 + \Delta^2)^{-1}, \tag{12}$$

which reduces to $C = g^2N/\kappa\gamma_\perp$ at resonance ($\Delta = 0$). The threshold pump rate is then $w_{\rm thr} = \gamma/(C - 1)$, which is valid for high temperatures. This equation shows that a cooperativity C greater than unity is needed and that, perhaps counterintuitively, when $C > 2$ the threshold pump rate is less than the spin-lattice relaxation rate. The mean inversion per spin is $\langle\sigma^z\rangle = 1/C$. For $C = 2$, spins in the ground state need only be pumped at half the spin-lattice relaxation rate (a single electron promoted from $|g\rangle$ to $|e\rangle$ changes the inversion by +2) to maintain the inversion or in equation form: $w\hat{\sigma}^-\hat{\sigma}^+ \geqslant \frac{1}{2}\gamma\hat{\sigma}^z$.

VII. PURCELL-ENHANCED EMISSION

Masing requires a collective cooperativity C greater than unity ($C > 1$), where C represents the collective strength of interaction between the spin ensemble and the cavity photon in the presence of spin dephasing and cavity decay. The cavity contribution to the cooperativity, g^2/κ, is proportional to the magnetic Purcell factor $\mathcal{F}_{\rm m} \propto Q/V_{\rm m}$ [26] which provides two important design criteria for the cavity: (i) maximize the spin-photon coupling g (minimize mode-volume $V_{\rm m}$) and (ii)

minimize the cavity decay rate κ (maximize the Q factor). The spin ensemble contribution $N/\gamma_\perp$ sets a requirement for maser gain media to have high spin concentration while maintaining low spin decoherence rates. Optimizing both quantities is challenging since increased spin densities typically results in increased spin dephasing due to higher probabilities of creating additional paramagnetic defects and impurities. For a diamond of volume V_s and spin concentration $n = N/V_s$ a minimum Purcell factor that satisfies $C > 1$ can be derived: $Q/V_m > (\gamma_\perp/nV_s)/\gamma_e^2\mu_0\hbar$. Cavity engineering of the Purcell factor is therefore the easiest route to collective cooperativity enhancement since spin ensemble properties can only be engineered to a limited extent, e.g., by isotopic purification.

VIII. CAVITY PHOTON POPULATION AND OUTPUT POWER

Using the steady-state equation for the collective inversion (4) and substituting Eq. (11) yields an expression for the cavity-mode photon population above threshold

$$n_c = \frac{1}{4}\left[\frac{wN}{\kappa} - \frac{\gamma_\perp}{g^2}(w+\gamma)(1+\Delta^2)\right] = \frac{N}{4\kappa C}[w(C-1)-\gamma]. \tag{13}$$

For high pump rates significantly above threshold ($w \gg w_{thr}$) and high collective cooperativity ($C \gg 1$) the cavity photon population is linearly dependent on the pump rate w and number of spins: $n_c \approx wN/4\kappa$. To extract microwave power from the maser, it is necessary to couple the cavity to an external waveguide or transmission line, quantified by the coupling factor β. The output power is proportional to the number of photons in the cavity, their energy and the rate at which they exit the cavity, according to $P_{out} = n_c\hbar\omega_c\kappa_e$. Substituting this expression into the cavity photon population Eq. (13) yields the output power:

$$P_{out} = \frac{1}{4}\hbar\omega_c\beta\kappa_0\left[\frac{wN}{(1+\beta)\kappa_0} - \frac{\gamma_\perp}{g^2}(w+\gamma)(1+\Delta^2)\right]. \tag{14}$$

The coupling β for which maximal output power is achieved can be found by differentiating with respect to β and solving for $\beta > 0$, yielding

$$\beta = \sqrt{\frac{1}{1+\gamma/w}\frac{1}{1+\Delta^2}\frac{g^2N}{\kappa_0\gamma_\perp}} - 1. \tag{15}$$

The optimal coupling depends on three different terms: the unsaturated inversion $\sigma^z = (1+\gamma/w)^{-1}$, a detuning term $(1+\Delta^2)^{-1}$ and a term resembling the collective cooperativity C that depends on the intrinsic cavity loss rate κ_0 instead of the total cavity loss rate κ. For diamond masers reported in the literature [6,27], $w/(w+\gamma) \simeq 0.2$ ($w \simeq 50$ s^{-1}, $\gamma \simeq 200$ s^{-1}) and $g^2N/\kappa_0\gamma_\perp \simeq 20$, leading to an optimal coupling of $\beta \sim 0.96$ which is very close to critical coupling. Figure 2 plots a map of output power as a function of β and w. For pump rates close to w_{thr} the optimal coupling is small and increases with increasing pump rate (see dashed line in Fig. 2). This is bounded by $\lim_{w\to\infty} w/(w+\gamma) = 1$ where the optimal coupling approaches $\lim_{w\to\infty}\beta = \sqrt{g^2N/\kappa_0\gamma_\perp} - 1$. The values for w_{thr} are in good agreement with recent experimental results and are about two orders of magnitude smaller than the values proposed in Ref. [16]. Higher pump rates will incur two penalties; (i) increased temperature of the diamond, which increases the spin-lattice relaxation rate γ and diminishes the effects of increased pump rates [27], and (ii) the spin decoherence rate $\gamma_\perp$ increases due to pumping and high spin-lattice relaxation rates. The effect on $\gamma_\perp$ can be assumed negligible since typical diamonds grown by chemical vapor deposition have T_2^* of the order of $\sim$1 μs therefore elevated pump rates $>10^4$ s^{-1} would be necessary to have an impact upon $\gamma_\perp$. We employ our model on a recently reported experimental maser threshold characterization in Ref. [27]. Figure 3 shows a comparison of experimental [Fig. 3(a)] and theoretical [Fig. 3(b)] output power as a function of w and β, using experimental parameters. The masing phase is reconstructed accurately, when considering a pump rate dependent spin-lattice relaxation rate due to heating effects. Peak output powers in the experiment are about -56 dBm, while the model produces a maximum of about -70 dBm. We attribute the difference to amplification effects [9], where thermal photons inside the cavity are amplified by spontaneous emission from the maser. Our first-order analytical model does not account for below threshold amplification effects. Second-order dynamical effects are required for the description, however, preventing a simple analytical expression. Nevertheless, our model can faithfully predict the maser phase and the coherent output power.

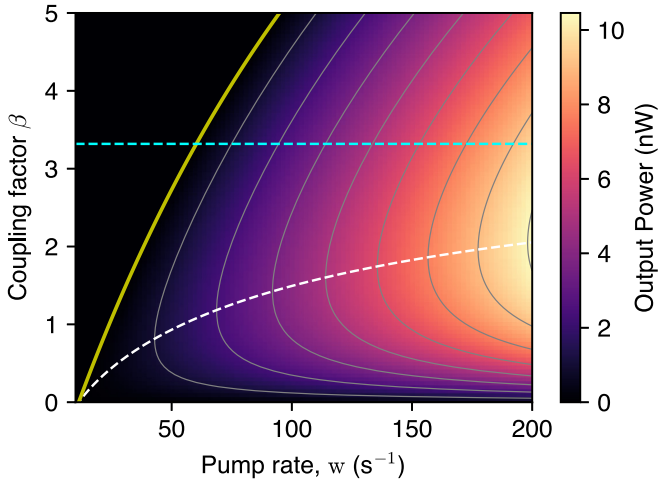

FIG. 2. Output power as a function of pump rate and coupling factor. Yellow line: Masing threshold. White dashed line: Coupling for optimal output power for given pump rate. Blue dashed line: Optimal coupling for infinite pump $\beta = \sqrt{C_0} - 1$. The cooperativity for unloaded cavity is $C_0 = 19$.

IX. SECOND-ORDER DYNAMICAL EQUATIONS

An exact expression for the rate of change of cavity photon number $n_c = \langle a^\dagger a\rangle$ can be derived from the Hamiltonian (1) and Liouvillian

$$\frac{d}{dt}\langle a^\dagger a\rangle = -2\kappa\,\langle a^\dagger a\rangle + 2\kappa\bar{n} + ig(\langle S^+ a\rangle - \langle a^\dagger S^-\rangle). \tag{16}$$

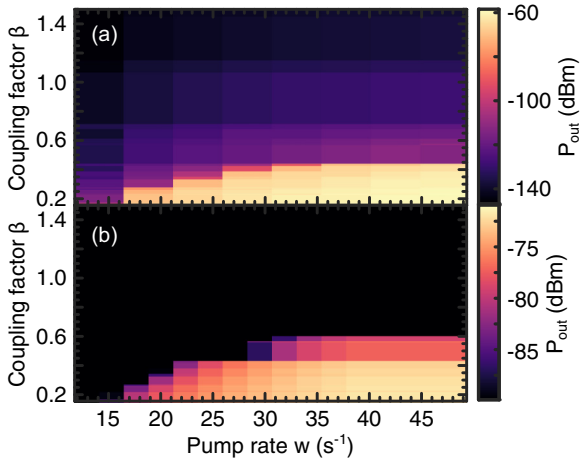

FIG. 3. Experimental and simulated output power as a function of optical pump rate and quality factor. (a) Experimental maser output power in logarithmic scale as presented in Ref. [27]. (b) Modeled P_{out} in logarithmic scale, using Eq. (14) with parameters from Ref. [27], as well as considering heating effects due to the laser pump.

The cavity field couples collectively to the spin polarization through the spin-photon coherence $\langle S^+a\rangle$ and its complex conjugate $\langle a^\dagger S^-\rangle$. The spin-photon coherence rate is

$$\frac{d}{dt}\langle S^+a\rangle = -(\kappa+\gamma_\perp+i\delta)\langle S^+a\rangle - ig\left(\frac{\langle S^z\rangle+N}{2}+\langle S^+S^-\rangle+\langle a^\dagger a\rangle\langle S^z\rangle\right), \quad (17)$$

where the third-order cumulant expansion is approximated as $\langle a^\dagger aS^z\rangle \simeq \langle a^\dagger a\rangle\langle S^z\rangle$ since the system is not driven or pumped by coherent fields so there is no defined phase (time invariant) ($\langle a\rangle = \langle a^\dagger\rangle = \langle S^\pm\rangle = 0$). $\delta = \omega_c - \omega_s$ is the cavity-spin detuning, decay terms due to spin-lattice relaxation and pumping are neglected since $\kappa, \gamma_\perp \gg w, \gamma$ and the number of spins assumed to be large, $N \gg 1$. The rate of change of the inversion $\langle S^z\rangle$ is exact:

$$\frac{d}{dt}\langle S^z\rangle = wN - (w+\gamma)\langle S^z\rangle - 2ig(\langle S^+a\rangle - \langle a^\dagger S^-\rangle), \quad (18)$$

and finally, the set of equations is closed by the spin-spin correlation (multipartite entanglement) $\langle S^+S^-\rangle = N^2\langle\sigma_i^+\sigma_j^-\rangle$:

$$\frac{d}{dt}\langle S^+S^-\rangle = -2\gamma_\perp\langle S^+S^-\rangle + ig\langle S^z\rangle(\langle S^+a\rangle - \langle a^\dagger S^-\rangle). \quad (19)$$

X. SPONTANEOUS, SUPERRADIANT, AND STIMULATED EMISSION

While maser oscillation is usually ascribed to stimulated emission, there are also spontaneous and superradiant emission processes. This can be seen by examining the final term of Eq. (16), the net photon emission into the cavity mode $\Gamma = ig(\langle S^+a\rangle - \langle a^\dagger S^-\rangle)$. Inserting the steady-state spin-photon coherence derived from Eq. (17) yields

$$\Gamma = \frac{2g^2}{\kappa+\gamma_\perp}\left(\frac{1}{1+\Delta^2}\right)\left(\frac{\langle S^z\rangle+N}{2}+\langle S^+S^-\rangle+\langle a^\dagger a\rangle\langle S^z\rangle\right). \quad (20)$$

The first term $\gamma_P = 2g^2/(\kappa+\gamma_\perp)$ is the Purcell-enhanced single-spin emission rate. The second term is a detuning factor and the final term sums the collective spontaneous, superradiant, and stimulated emission into the cavity. Using parameters previously reported for diamond masers [6,27] ($n_c \equiv \langle a^\dagger a\rangle \simeq 10^8$, $N \simeq 4\times10^{13}$, $\kappa \simeq 10^6$ s^{-1}, $\gamma_\perp \simeq 2\times10^6$ s^{-1}, $g \simeq 0.7$ s^{-1}, $\Delta = 0$) yields a Purcell rate of $\gamma_P \sim 3\times10^{-7}$ s^{-1} and a collective spontaneous emission rate of $\Gamma_{sp} = \gamma_P(\langle S^z\rangle+N)/2 \approx 7\times10^6$ s^{-1}. Far above threshold where $n_c \gg \bar{n}$ an estimate for the steady-state emission can be derived from Eq. (16): $\Gamma_{ss} \simeq 2\kappa n_c$. Together with the clamped inversion $\langle S^z\rangle_{ss} = \kappa\gamma_\perp/g^2$ and Eq. (19), the steady-state superradiant emission rate can be calculated: $\Gamma_{SR} \simeq \gamma_P\langle S^+S^-\rangle_{ss} \approx \gamma_P(\kappa^2/g^2)n_c \approx 6.6\times10^{13}$ s^{-1}. The stimulated emission rate is $\Gamma_{st} = \gamma_P\langle a^\dagger a\rangle\langle S^z\rangle = \gamma_P(\kappa\gamma_\perp/g^2)n_c \approx 1.3\times10^{14}$ s^{-1}. The spontaneous emission rate is seven orders of magnitude smaller than the other emission processes and is also smaller than the thermal photon emission rate at room temperature ($2\kappa\bar{n} \sim 10^9$ s^{-1}), so can be neglected. However, it is noteworthy that superradiant emission accounts for one third of the total emission and that the fractions of superradiant and stimulated emission are $\kappa/(\kappa+\gamma_\perp)$ and $\gamma_\perp/(\kappa+\gamma_\perp)$, respectively. If $\kappa \ll \gamma_\perp$ the maser is in the good-cavity regime where coherence is mostly stored in the cavity and stimulated emission is dominant. Conversely, if $\kappa \gg \gamma_\perp$ the maser is in the bad-cavity regime where coherence is mostly stored in the spin ensemble and superradiance is dominant. In the intermediate regime where $\kappa \sim \gamma_\perp$ the coherence is stored equally in both the cavity and the spin-ensemble and superradiant and stimulated contribute equally to the emission rate.

XI. CONCLUSION AND OUTLOOK

The presented theoretical analysis of steady-state maser dynamics provides an accessible framework for further room-temperature maser research. Our discussion is based on a Lindbladian master equation approach from which we derive the first and second-order time dependence of expectation values for spin inversion, spin-spin, and spin-photon correlations, and the cavity photon number. For the steady-state we find analytic expressions which could form the basis of design rules for masers operating at room temperature and can be easily extended to any temperature. Finally, we highlight that maser photon emission is not solely governed by stimulated emission, but is accompanied by a significant amount of superradiance. The difference between a good cavity and a bad cavity limit is identified by the ratio of cavity loss rate κ and spin dephasing rate $\gamma_\perp$. These results provide a comprehensive theory that enables the conception of new experiments to explore and improve the state-of-the-art in maser technology.

ACKNOWLEDGMENTS

We gratefully acknowledge funding from the Royal Society (Grant No. URF/R1/191297) and the UK Engineering and Physical Sciences Research Council (Grant No. EP/S000798/2).

APPENDIX

Here, we present in detail the construction of a rate equation model for the multienergy level scheme of NV centers in diamond and consecutive mapping onto a two-level model.

1. NV center population dynamics under optical pumping

The dynamics of the eight sublevels involved in the optical pumping process of a single NV center subjected to an optical pump of rate w_{opt} can be written

$$\frac{d}{dt}\mathbf{R} = \mathbf{M}\mathbf{R},$$

where

$$\mathbf{R} = [-1_g \quad 0_g \quad +1_g \quad -1_e \quad 0_e \quad +1_e \quad {}^1A_1 \quad {}^1E]^{\mathrm{T}}$$

is a vector whose components are the probabilities (populations) of finding an electron in a particular state and

$$\mathbf{M} = \begin{bmatrix}
-w_{\text{opt}} - \frac{1}{2}(\gamma+\gamma') & \frac{1}{2}\gamma & \frac{1}{2}\gamma' & \Gamma & 0 & 0 & 0 & k_{81} \\
\frac{1}{2}\gamma & -w_{\text{opt}} - \frac{1}{2}(\gamma+\gamma'') & \frac{1}{2}\gamma'' & 0 & \Gamma & 0 & 0 & k_{82} \\
\frac{1}{2}\gamma' & \frac{1}{2}\gamma'' & -w_{\text{opt}} - \frac{1}{2}(\gamma'+\gamma'') & 0 & 0 & \Gamma & 0 & k_{83} \\
w_{\text{opt}} & 0 & 0 & -\Gamma - k_{47} & 0 & 0 & 0 & 0 \\
0 & w_{\text{opt}} & 0 & 0 & -\Gamma - k_{57} & 0 & 0 & 0 \\
0 & 0 & w_{\text{opt}} & 0 & 0 & -\Gamma - k_{67} & 0 & 0 \\
0 & 0 & 0 & k_{47} & k_{57} & k_{67} & -k_{78} & 0 \\
0 & 0 & 0 & 0 & 0 & 0 & k_{78} & -(k_{81}+k_{82}+k_{83})
\end{bmatrix}$$

is a matrix that couples the sublevels with transition rates, where w_{opt} is the NV center optical pump rate, Γ is the excited triplet state fluorescent lifetime, γ, γ', and γ'' are the (high-temperature) spin-lattice relaxation rates between the ground-state triplet sublevels, k_{47}, k_{57}, k_{67} are the intersystem crossing rates from the excited state triplets to ${}^1A_1$, k_{78} is the singlet decay rate from ${}^1A_1$ to ${}^1E$ and k_{81}, k_{82}, k_{83} are the nonradiative decay rates from ${}^1E$ to the $|-1\rangle, |0\rangle, |+1\rangle$ ground-state triplet sublevels, respectively. The steady-state populations of the eight sublevels can be found by solving the linear homogeneous matrix equation $\mathbf{MR} = 0$. Values for the rate parameters used in the main text are given in Table I. Figure 4 presents results from solving the matrix equation for the inversion σ^z, corresponding to the population difference between 0_g and -1_g. The two solid lines are results with and without assuming a finite mixing of the triplet sublevels.

TABLE I. Values for rate parameters used in full eight-level pumping dynamics of a single NV center.

Parameter	Ref. [28]
Γ	$65.9\,\mu\text{s}^{-1}$
γ	$200\ \text{s}^{-1}$
γ'	$200\ \text{s}^{-1}$
γ''	$200\ \text{s}^{-1}$
k_{47}	$53.3\,\mu\text{s}^{-1}$
k_{57}	$7.9\,\mu\text{s}^{-1}$
k_{67}	$53.3\,\mu\text{s}^{-1}$
k_{78}	$1\ \text{ns}^{-1}$
k_{81}	$0.7\,\mu\text{s}^{-1}$
k_{82}	$1.0\,\mu\text{s}^{-1}$
k_{83}	$0.7\,\mu\text{s}^{-1}$

The mixing results in changes of intersystem crossing rates, specifically a finite rate k_{57}. This can be caused by a misalignment of the magnetic field to the NV^- defect axis. The inversion from a full eight sublevel model can be mapped onto an effective two-level system. As described in the main text, the inversion is given by $\sigma^z = \xi(1+\gamma/\eta w_{\text{opt}})^{-1}$, where η represents the pump efficiency between the effective pump

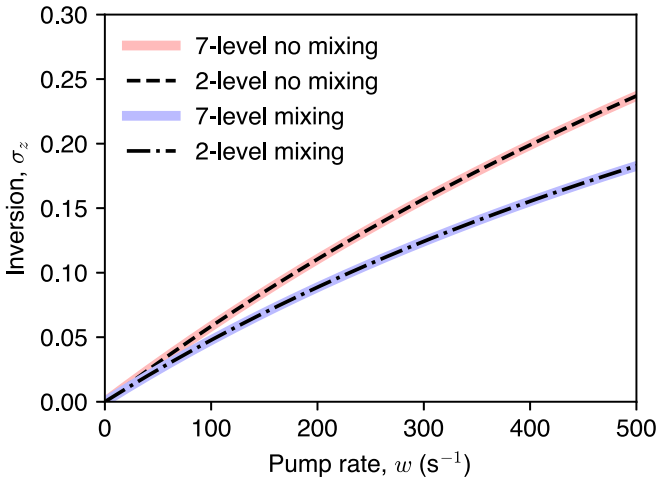

FIG. 4. Inversion σ^z for optical pump rate w_{opt}. Inversion as a function of optical pump rate obtained from the full eight sublevel rate equation model (solid lines) and by optimizing a simplified two-level model to the results of the full model (dashed lines). No and a finite triplet state mixing was assumed (red, dashed and blue, dash-doted lines, respectively), represented by $k_{57} = 0\,\mu\text{s}^{-1}$ and $k_{57} = 7.9\,\mu\text{s}^{-1}$. State mixing results in a reduced maximal achievable inversion.

rate w of the two-level system and the applied optical pump rate w_{opt} and a scaling parameter ξ accounting for the state mixing. Both parameters can be determined by fitting the simplified inversion to the full eight sublevel model. Comparing both models, we find that the simple two-level system (dashed lines in Fig. 4) can fully reproduce the eight sublevel model. The pump efficiency η and mixing scale ξ were found to be $\eta = 0.124$ for zero mixing and $\eta = 0.166$ and $\xi = 0.623$ for nonzero mixing due to a $7.9\,\mu\mathrm{s}^{-1}$ transition rate between the excited $m_s = 0$ state and the singlet $^1A_1$ [28].

[1] J. P. Gordon, H. J. Zeiger, and C. H. Townes, Molecular microwave oscillator and new hyperfine structure in the microwave spectrum of NH_3, Phys. Rev. **95**, 282 (1954).

[2] F. Riehle, Microwave frequency standards, in *Frequency Standards* (John Wiley & Sons, New York, 2003), Chap. 8, pp. 229–253.

[3] R. F. C. Vessot, The atomic hydrogen maser oscillator, Metrologia **42**, 468 (2005).

[4] D. M. Arroo, N. M. Alford, and J. D. Breeze, Perspective on room-temperature solid-state masers, Appl. Phys. Lett. **119**, 140502 (2021).

[5] M. Oxborrow, J. D. Breeze, and N. M. Alford, Room-temperature solid-state maser, Nature (London) **488**, 353 (2012).

[6] J. D. Breeze, E. Salvadori, J. Sathian, N. M. Alford, and C. W. Kay, Continuous-wave room-temperature diamond maser, Nature (London) **555**, 493 (2018).

[7] M. Jiang, Y. Qin, X. Wang, Y. Wang, H. Su, X. Peng, and D. Budker, Floquet spin amplification, Phys. Rev. Lett. **128**, 233201 (2022).

[8] A. Sherman, L. Buchbinder, S. Ding, and A. Blank, Performance analysis of diamond-based masers, J. Appl. Phys. **129**, 144503 (2021).

[9] T. Day, M. Isarov, W. J. Pappas, B. C. Johnson, H. Abe, T. Ohshima, D. R. McCamey, A. Laucht, and J. J. Pla, Room-temperature solid-state maser amplifier, Phys. Rev. X **14**, 041066 (2024).

[10] D. P. Fahey, K. Jacobs, M. J. Turner, H. Choi, J. E. Hoffman, D. Englund, and M. E. Trusheim, Steady-state microwave mode cooling with a diamond N-V ensemble, Phys. Rev. Appl. **20**, 014033 (2023).

[11] A. Blank, A. Sherman, B. Koren, and O. Zgadzai, An anti-maser for mode cooling of a microwave cavity, J. Appl. Phys. **134**, 214401 (2023).

[12] W. Ng, H. Wu, and M. Oxborrow, Quasi-continuous cooling of a microwave mode on a benchtop using hyperpolarized NV^- diamond, Appl. Phys. Lett. **119**, 234001 (2021).

[13] Y. Zhang, Q. Wu, H. Wu, X. Yang, S.-L. Su, C. Shan, and K. Mølmer, Microwave mode cooling and cavity quantum electrodynamics effects at room temperature with optically cooled nitrogen-vacancy center spins, npj Quantum Inf. **8**, 125 (2022).

[14] H. Wu, S. Mirkhanov, W. Ng, and M. Oxborrow, Bench-top cooling of a microwave mode using an optically pumped spin refrigerator, Phys. Rev. Lett. **127**, 053604 (2021).

[15] A. Gottscholl, M. Wagenhöfer, V. Baianov, V. Dyakonov, and A. Sperlich, Room-temperature silicon carbide maser: Unveiling quantum amplification and cooling, arXiv:2312.08251.

[16] L. Jin, M. Pfender, N. Aslam, P. Neumann, S. Yang, J. Wrachtrup, and R.-B. Liu, Proposal for a room-temperature diamond maser, Nat. Commun. **6**, 1 (2015).

[17] M. W. Doherty, N. B. Manson, P. Delaney, F. Jelezko, J. Wrachtrup, and L. C. L. Hollenberg, The nitrogen-vacancy colour centre in diamond, Phys. Rep. **528**, 1 (2013).

[18] E. Fraczek, V. G. Savitski, M. Dale, B. G. Breeze, P. Diggle, M. Markham, A. Bennett, H. Dhillon, M. E. Newton, and A. J. Kemp, Laser spectroscopy of NV^- and NV^0 colour centres in synthetic diamond, Opt. Mater. Express **7**, 2571 (2017).

[19] J.-P. Tetienne, L. Rondin, P. Spinicelli, M. Chipaux, T. Debuisschert, J.-F. Roch, and V. Jacques, Magnetic-field-dependent photodynamics of single NV defects in diamond: An application to qualitative all-optical magnetic imaging, New J. Phys. **14**, 103033 (2012).

[20] A. Patel, Z. Chowdhry, A. Prabhakar, A. Rathi, and V. P. Bhallamudi, Single and double quantum transitions in spin-mixed states under photo-excitation, Sci. Rep. **14**, 22421 (2024).

[21] R. H. Dicke, Coherence in spontaneous radiation processes, Phys. Rev. **93**, 99 (1954).

[22] M. Tavis and F. W. Cummings, Exact solution for an N-molecule—radiation-field Hamiltonian, Phys. Rev. **170**, 379 (1968).

[23] A. Jarmola, V. M. Acosta, K. Jensen, S. Chemerisov, and D. Budker, Temperature- and magnetic-field-dependent longitudinal spin relaxation in nitrogen-vacancy ensembles in diamond, Phys. Rev. Lett. **108**, 197601 (2012).

[24] F. Arecchi and R. Bonifacio, Theory of optical maser amplifiers, IEEE J. Quantum Electron. **1**, 169 (1965).

[25] B. McNeil, Due credit for Maxwell–Bloch equations, Nat. Photon. **9**, 207 (2015).

[26] J. Breeze, K.-J. Tan, B. Richards, J. Sathian, M. Oxborrow, and N. M. Alford, Enhanced magnetic purcell effect in room-temperature masers, Nat. Commun. **6**, 6215 (2015).

[27] C. W. Zollitsch, S. Ruloff, Y. Fett, H. T. Wiedemann, R. Richter, J. D. Breeze, and C. W. Kay, Maser threshold characterization by resonator Q-factor tuning, Commun. Phys. **6**, 295 (2023).

[28] J. Klatzow, J. N. Becker, P. M. Ledingham, C. Weinzetl, K. T. Kaczmarek, D. J. Saunders, J. Nunn, I. A. Walmsley, R. Uzdin, and E. Poem, Experimental demonstration of quantum effects in the operation of microscopic heat engines, Phys. Rev. Lett. **122**, 110601 (2019).